Comparison of the electronic structures and energetics of ferroelectric $LiNbO_3$ and $LiTaO_3$

Iris Inbar and R. E. Cohen
Carnegie Institution of Washington, Geophysical Laboratory, 5251 Broad Branch Road, N.W., Washington, D.C. 20015
(Received 3 August 1995)

Extensive linearized augmented plane-wave frozen phonon calculations were performed in order to understand the origin of ferroelectricity in $LiTaO_3$ and $LiNbO_3$. Displacement of the Li atoms alone results in an anharmonic single well, whereas displacements of oxygen and lithium together result in deep double wells, much deeper than the transition temperatures, T_c. This is contrary to current theories which model the underlying potential as a triple well potential for the lithium atoms. Our results support an order-disorder model for the oxygen atoms as the driving mechanism for the ferroelectric instability. Oxygen displacements alone against the transition-metal atoms result in shallower double wells as a result of oxygen-lithium overlap so that the lithium and oxygen displacements are strongly coupled. We find large hybridization between the oxygens and the transition-metal atoms. Thus ferroelectricity in the $Li(Nb,Ta)O_3$ system is similar in origin to ferroelectricity in the perovskites. We also find that the electronic structures of $LiTaO_3$ and $LiNbO_3$ are very similar and hardly change during the phase transition.

I. INTRODUCTION

The origin of ferroelectricity in the two well-known ferroelectric systems, $LiNbO_3$ and $LiTaO_3$, has been subject to intense study since the discovery of $LiNbO_3$ in 1949.[1] They have many applications in optical, electro-optical, and piezoelectric devices, but the fundamental physics that leads to their ferroelectric behavior have not been studied. Their transition temperatures, which are among the highest known ferroelectric transition temperatures, are quite different, 1480 K for $LiNbO_3$ and 950 K for $LiTaO_3$. The electronic origin of their different T_c is a mystery since Nb^{5+} and Ta^{5+} behave very similarly, and structurely these materials are almost identical. The origin of their ferroelectric instability as well as their different transition temperatures is investigated.

Both materials undergo only one structural phase transition. The paraelectric structure has a 10-atom unit cell and the average structure belongs to the $R\bar{3}c$ space group, The atomic arrangement consists of oxygen octahedra sharing faces along the polar trigonal axis. The transition-metal atoms occupy the centers of oxygen octahedra, and the average Li atom position lies on the face between two adjacent oxygen octahedra [Fig. 1(a)]. The ferroelectric structure is rhombohedral, and belongs to the space group $R3c$. The transition-metal atom is displaced from the center of the oxygen octahedra along the trigonal axis. The next oxygen octahedron along this axis is empty and the adjacent octahedron has a Li atom ferroelectrically displaced from the oxygen face in the spontaneous polarization P_s direction [Fig. 1(b)]. Glass in 1968 and later Johnston and Kaminow have determined, using dielectric and thermal measurements, that the phase transformation in these systems is continuous.[2,3]

Whether the transition is displacive or order-disorder has been much discussed and confusion abounds. A displacive phase transition is one where the local potential in the mean field of the rest of the crystal has a single minimum, and is characterized by a temperature-dependent optic mode approaching zero as the temperature reaches T_c. Temperature dependence measurements of Raman, Rayleigh scattering,[3] and infrared reflectivity,[4–6] show soft mode behavior for one polar A_1 (TO) optic mode in the ferroelectric phase. This soft mode crosses many E modes (whose eigenvectors give ionic displacements perpendicular to the polar axis), and thus this specific mode is difficult to trace in detail. Tomeno and Matsumura[7] measured the dielectric constants of $LiTaO_3$ and found a large Curie constant, and interpreted their results as indicative of a displacive transition.

Evidence for the transition having an order-disorder character came from Penna and co-workers,[8–11] who observed no mode softening for $LiTaO_3$ for the A_1 (TO) mode, followed by Chowdhury, Peckham, and Saunderson[12] who performed neutron scattering experiments on $LiNbO_3$, and also failed to observe any softening of the A_1 mode. Okamoto, Wang, and Scott[13] used Raman scattering to study $LiNbO_3$ between room temperature and 1225 K and saw two of the three A_1 modes (which are, at room temperature, TO, LO, and TO at 250, 270, and 274 cm^{-1}, respectively), and observed anomalous behavior for one of them (at 274 cm^{-1}) as the temperature reached T_c. They noted that the decrease in the peak frequency was mostly due to the rapid increase in

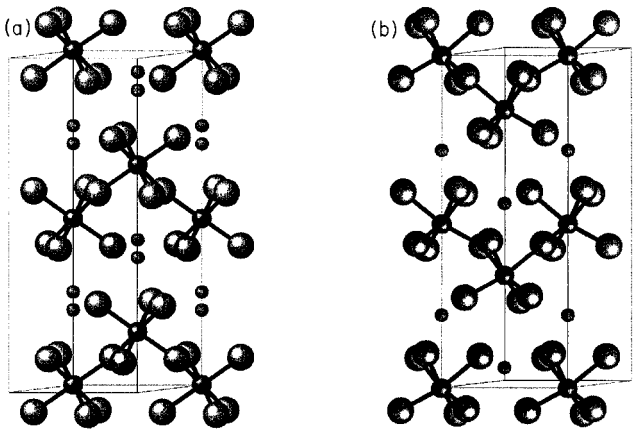

FIG. 1. The (a) paraelectric and (b) ferroelectric structures of $LiTaO_3$ and $LiNbO_3$. The hexagonal unit cell is outlined.

damping as the linewidth had a divergent form in temperature, whereas the quasiharmonic frequency remained almost temperature independent. Their conclusion was therefore that $LiNbO_3$ does not exhibit a typical displacive transition, but rather resembles an order-disorder system. Zhang and Scott[14] reported these measurements on $LiTaO_3$, and found the same kind of behavior. In an order-disorder phase transition the local potential is characterized by a double (or more) well, with the thermal energy kT_c much smaller than the well depth and no soft phonon mode exist since phonons now oscillate within each well and the wells remain essentially unchanged throughout the phase transition. These transitions are characterized by a diffusive soft mode that is not a phonon but represent large-amplitude thermal hopping between the wells. At T above T_c the crystal is nonpolar in a thermally averaged sense.

Jayaraman and Ballman[15] argued for an order-disorder-type transition because they saw little pressure dependence of the Raman mode; they also emphasize the difference from ferroelectric perovskites, which show a strong pressure dependence. Raptis[16] measured and analyzed Raman modes of $LiTaO_3$ between room temperature and 1200 K and observed softening of this A_1 mode (along with others) to a certain degree. However, the decrease was characterized with an order-disorder model. Catchen and Spaar[17] used perturbed-angular-correlation (PAC) spectroscopy to measure nuclei-electric-quadrupole interactions at the Li sites over a temperature range of 295–1100 K, and Cheng *et al.*[18] studied inelastic neutron scattering from room temperature up to 800 °C (1100 K) in $LiTaO_3$; both failed to observe mode softening, therefore not supporting the displacive picture for the phase transition. Tezuka, Shin, and Ishigame[19] used hyper-Raman and Raman spectra of $LiTaO_3$ between 14 and 1200 K. No evidence was found for the softening of the A_1 mode; however, a strong Debye-type relaxational mode was found in the two phases, suggesting an order-disorder-type transition. They interpreted the anomalous line shape of an A_1 mode in terms of coupling with relaxational modes.

Most ferroelectric systems are thought of as exhibiting displacive behavior far from the transition temperature region and order-disorder characteristics near T_c. In the $Li(Nb,Ta)O_3$ systems this conclusion is supported by a number of studies.[20–22]

In other ferroelectric oxides, like the perovskites $KTaO_3$ and $KNbO_3$, the mechanism behind the phase transition has also been debated. Evidence for the transition being of the displacive type are presented by Nunes, Axe, and Shirane[23] and Samara,[24] while Comes, Lambert, and Guinier[25] and PAC experiments by Dougherty *et al.*[26] point to it being of the order-disorder type. Sokoloff, Chase, and Rytz[27] have studied Raman scattering of $KNbO_3$ and $BaTiO_3$ and discovered central peaks that have line shapes and thermal dependence characteristics of Debye relaxation modes as well as symmetry properties consistent with the eight-site model. A theoretical study by Edwardson of $KNbO_3$,[28] using interacting polarizable ions in static and dynamic simulations found a mixture of order-disorder and displacive type behavior. Postnikov *et al.*[29,30] carried out a linear muffin-tin orbital LMTO study examining the total energy of $KNbO_3$ in the tetragonal and rhombohedral phases. These calculations found that displacing the Nb atom along the $\langle 100 \rangle$ direction from its tetragonal cell position corresponds to a saddle point on the total-energy surface. This becomes a minima when the lattice strain is included. They have also carried out total energy calculations for $KTaO_3$ and found no ferroelectric instability for the calculated volume. They were able to induce a phase transition by applying negative pressure (expanding the lattice). An x-ray absorption fine-structure study of KTN by Hanske-Petitpierre *et al.*[31] found that the ferroelectric transition is not displacive and involves orientational order-disorder transition of the Nb atom. A recent first principles investigation of eight perovskites[32,33] suggests that in materials like $KNbO_3$ and $BaTiO_3$, which are rhombohedral at $T=0$, the sequence of successive transitions is explained via the eight-site model, where the order parameter in the paraelectric phase fluctuates between the eight minima in the [111] directions. These sites are minima at the cubic phase, before the development of the strain.

The theories developed thus far for the $LiTaO_3$ and $LiNbO_3$ systems usually are based on the Lines model.[34] Lines applied his effective-field theory to $LiTaO_3$, and parametrized it as a displacive ferroelectric due to the data available at the time by Johnston and Kaminow,[3] and assumed a triple well potential for the Li atoms. Abrahams *et al.*[35] performed neutron scattering of $LiTaO_3$ between room temperature and 940 K, and discovered that, above T_c, the lithium-atom positions in $LiTaO_3$ become disordered and hop among the centrosymmetric position and sites at $\pm$ 0.37 Å along the optic axis. Similar measurements for $LiNbO_3$ show the same kind of behavior.[36] The neutron scattering data are the cornerstone behind all theories modeling this ferroelectric transition as an order-disorder mechanism with the Li ions hopping among the centrosymmetric sites and the adjacent octahedral sites. This approach was adopted by Birnie,[37–39] who modeled the Li hopping as a Frenkel defect, and later by Bakker, Hunsche, and Kurz,[40] who used these data in addition to the triple-well Lines model as a basis for a quantum-mechanical description of the phase transformation in $LiTaO_3$. Bakker, Hunsche, and Kurz predicted and observed[41] a 32-cm^{-1} excitation, which they ascribed to Li motions between the central and lowest wells. This excitation frequency has not been observed in other studies, however.[42]

II. METHOD

The Kohn-Sham equations[43,44] are solved self-consistently using the full potential linearized augmented plane-wave (LAPW) method,[45] where the electronic many-body exchange-correlation interactions are described by the local density approximation using Hedin-Lundqvist parametrization.[46] There are no shape approximations for the charge density or the potential. This method has proved predictive in many previous studies. Examples include the prediction of a high-pressure phase transformation in silica,[47] studies of iron at high pressures,[48,49] studies of Al_2O_3,[50] MgO and CaO,[51] $MgSiO_3$,[52] and high-temperature superconductors.[53] This method was previously applied successfully to perovskite ferroelectrics like $BaTiO_3$, $PbTiO_3$,[54] and $KNbO_3$.[55]

We use the LAPW+LO method,[56] which uses a mixed basis consisting of the LAPW basis plus extra localized or-

bitals inside the muffin-tin spheres. The extra local orbitals remove a Li *s* ghost state and relax the valence states. It also allows us the use of a single energy window. Local orbitals included *s* for Li, *s* and *p* for O, and *s*, *p*, and *d* for the Nb and Ta atoms. Other details of the calculations include a muffin tin size of 1.6 bohrs for the Li and 2.0 Bohr for the Nb and Ta atoms. The oxygen's muffin-tin radius was 1.6 bohrs for oxygen-Nb separation up to 1.882 Å (3.556 bohrs). The corresponding distance in $LiTaO_3$ is O-Ta up to 1.8845 Å (3.562 bohrs). At this point the oxygen muffin-tin radius was decreased to 1.552 bohrs. For smaller separations the muffin-tin radius was 1.506 bohrs. In order to be able to compare the energies calculated using different muffin-tin radii, we have repeated calculations with the three sets of muffin-tin radii to find the energy shift due to this change in the muffin-tin radii, and have assumed that this small shift ($\sim$ 7 mRy) is constant for small displacements of atoms.

A $4\times4\times4$ special *k*-point mesh was used, which generates a total of 10 *k* points in the irreducible zone. To test energy convergence, the energies at the symmetric and experimental structures of both $LiTaO_3$ and $LiNbO_3$ were also calculated with a $6\times6\times6$ mesh, which generates 28 *k* points in the irreducible zone, and these energies are shown in Table I. The change in energy difference for the two *k*-point sets between the experimental and the symmetric configurations is 0.069 mRy for $LiNbO_3$ and 0.3 mRy for $LiTaO_3$, demonstrating convergence.

The $RK_{\max}$ parameter was set to 7.0, which gives approximately 1150 basis functions for the $LiTaO_3$ calculations and 1050 functions for $LiNbO_3$. The core states were calculated fully relativistically and the valence states semirelativistically. For each Ta atom, the states up to $4f$ were included in the core, and as a result 0.588 electron extended beyond the muffin-tin sphere. For each Nb atom states up to $4s$ were included in the core and only 0.07 core electron extended beyond the sphere; core electrons that spill out of the muffin tins see an extrapolated spherical core potential. Also, in $LiNbO_3$ the Li atom *s* states were included as bands, whereas in $LiTaO_3$ they were treated as core states.

III. RESULTS AND DISCUSSION

A. Energetics

We have calculated the potential-energy surfaces along the experimental soft-mode coordinate. To test the sensitivity to the different lattice parameters, the total energy of $LiNbO_3$ was calculated in the ferroelectric configuration using both the $LiNbO_3$ lattice parameters (a_H=5.14829 Å and c_H=13.8631 Å),[57] and the $LiTaO_3$ lattice parameters (a_H=5.15428 Å and c_H=13.78351 Å),[35] a difference of 0.75% in the *c/a* ratio. The effect of this strain on the total energies was almost negligible; slightly less than 1 mRy or 5.5% of the well depth. This is in contrast to the case of the perovskites; e.g., $PbTiO_3$, where a strong dependence of the total energy on the tetragonal strain was observed, and the energy decreases markedly, about 35% of the well depth for the experimental 6% *c/a* strain.[54] Also the total energy of $LiNbO_3$ using both the experimental $LiNbO_3$ atomic positions [Li at (0.2829,0.2829,0.2829), Nb at (0,0,0), and O at (0.1139,0.3601,−0.2799)] (Ref. 57) and the $LiTaO_3$ atomic positions [Li at (0.279,0.279,0.279), Ta at (0,0,0), and O at (0.1188,0.3622,−0.2749) (Ref. 35)] were calculated. The resulting wells are less than 1 mRy different, the $LiNbO_3$ atomic positions yielding the deeper well. For the purpose of comparison, except for a few more points that yielded the same results (energy differences of less than 1 mRy), all points were calculated using the experimental lattice parameters and positions of $LiTaO_3$ to facilitate comparison of the effects of chemistry on ferroelectric behavior and electronic structure. Table I summarizes the results for $LiTaO_3$ and $LiNbO_3$. The first column refers to the displaced atoms, and to the amount of displacement as a fraction of the paraelectric to experimental ferroelectric normal-mode amplitude. Note that one distortion of $LiTaO_3$ published earlier[58] was not along the soft-mode coordinate; the present results correct this error.

Figure 2(a) shows the potential-energy surfaces of $LiTaO_3$ with respect to displacements of Li only (upper curves), O only (middle, shallow double wells) and Li+O (lower curves). Figure 2(b) shows the same picture for $LiNbO_3$. The lithium displacements along the soft-mode coordinate result in a single anharmonic well with low curvature. Displacing only the oxygens against the transition-metal atoms results in shallow double wells, and the deep double wells are the result of the Li+O displacements along the experimental ferroelectric coordinate.

The wells resulting from the oxygen and lithium displacements have well depths of 17.3 mRy (2739 K) and 18.3 mRy (2858 K) for $LiTaO_3$ and $LiNbO_3$, respectively. Both wells are much deeper than the experimental transition temperatures, which is consistent with an order-disorder character for the phase transition.

The energy was fit to a fourth-order polynomial in normal mode amplitude, $Q=\sqrt{\Sigma_i m_i u_i^2}$. The Schrödinger equation was solved numerically to obtain the eigenstates assuming one-dimensional noninteracting anharmonic oscillators along the soft-mode coordinate. Figure 3 shows the energy surface as a function of the normal-mode amplitude, *Q*, and the energy levels. We can see that the two wells have a different shape due to the factor of about 2 in mass of Nb and Ta, and thus the Nb approximately displaces twice as much as the Ta relative to the center of mass, which results in a different normal-mode amplitude *Q*. The energy difference between the ground and lowest excited state gives a frequency for $LiTaO_3$ of 270 cm^{-1} in fairly good agreement with the experimental Raman frequency of 201–225 cm^{-1} considering the one-dimensional noninteracting oscillator approximation. For $LiNbO_3$, the calculated frequency is 250 cm^{-1}, in excellent agreement with experimental data of about 250–275 cm^{-1}.

These results indicate that these structural phase transitions are *not* dominated energetically by the displacements of the lithium alone. The potential-energy surfaces show that the deep double wells are the result of the *coupled* motion of lithiums and oxygens. Displacement of the lithiums alone hardly changes the energy of the system. This is in contrast to current theories, which model the displacement of the lithiums as the driving mechanism for the ferroelectric instability.

In order to understand the oxygen-lithium coupling, we calculated the dynamical matrices for the LAPW and Madelung energies (assuming fully charged ions) for both materi-

TABLE I. Total energies for different configurations for $LiNbO_3$ and $LiTaO_3$. Coordinates are in primitive rhombohedral coordinates. The first column refers to the displaced atom and the amount of displacement as a fraction of the paraelectric to experimental ferroelectric normal-mode amplitude.

Atomic positions	Li	O	E(Ryd+16193)
		$LiNbO_3$	
Paraelectric	0.25,0.25,0.25	0.136,0.363,−0.25	−0.8462
			−0.8464[a]
Li - 0.5	0.2645,0.2645,0.2645	0.136,0.363,−0.25	−0.8465
Li - 1.0	0.279,0.279,0.279	0.136,0.363,−0.25	−0.8467
Li - 1.55	0.295,0.295,0.295	0.136,0.363,−0.25	−0.8422
O - 0.75	0.25,0.25,0.25	0.1231,0.3624,−0.2687	−0.8502
O - 1.05	0.25,0.25,0.25	0.1179,0.3621,-0.2761	−0.8498
O - 1.3	0.25,0.25,0.25	0.1135,0.3615,−0.2874	−0.8473
O+Li - 0.5	0.2645,0.2645,0.2645	0.1276,0.3629,−0.2625	−0.8539
O+Li - 0.75	0.272,0.272,0.272	0.1231,0.3624,−0.2687	−0.8586
O+Li - 1.0[b]	0.279,0.279,0.279	0.1188,0.3622,−0.2749	−0.8638
			−0.8644[a]
O+Li - 1.05	0.2804,0.2804,0.2804	0.1179,0.3621,−0.2761	−0.8643
O+Li - 1.3	0.288,0.288,0.288	0.1135,0.3618,−0.2834	−0.8639[c]
O+Li - 1.5	0.294,0.294,0.294	0.1099,0.3615,−0.2874	−0.8579[d]
Atomic positions	Li	O	E (Ryd+ 63395)
		$LiTaO_3$	
Paraelectric	0.25,0.25,0.25	0.136,0.363,−0.25	−0.07834
			−0.07830 [a]
Li - 0.5	0.2645, 0.2645,0.2645	0.136,0.363,−0.25	−0.0784
Li - 1.0	0.279,0.279,0.279	0.136,0.363,−0.25	−0.0778
Li - 1.55	0.295,0.295,0.295	0.136,0.363,−0.25	−0.0716
O - 0.75	0.25,0.25,0.25	0.1231,0.3624,−0.2687	−0.0843
O - 1.05	0.25,0.25,0.25	0.1179,0.3621,−0.2761	−0.0806
O - 1.3	0.25,0.25,0.25	0.1135,0.3615,−0.2874	−0.0719
O+Li - 0.5	0.2645,0.2645,0.2645	0.1276,0.3629,−0.2625	−0.0898
O+Li - 0.75	0.272,0.272,0.272	0.1231,0.3624,−0.2687	−0.0939
O+Li - 1.0[b]	0.279,0.279,0.279	0.1188,0.3622,−0.2749	−0.0957
			−0.0960 [a]
O+Li - 1.05	0.2804,0.2804,0.2804	0.1179,0.3621,−0.2761	−0.0954
O+Li - 1.3	0.288,0.288,0.288	0.1135,0.3618,−0.2834	−0.0914 [e]
O+Li - 1.5	0.294,0.294,0.294	0.1099,0.3615,−0.2874	−0.0809 [f]

[a]Calculated using 28 k points in the irreducible Brillouin zone to test convergence. Other points included 10 k points.

[b]This is the experimental ferroelectric disortion.

[c]Energy shift due to different muffin-tin sizes is included as described in the text. Energy shift is 6.64 mRy.

[d]Energy shift due to different muffin-tin sizes is 6.6 mRy.

[e]Energy shift due to different muffin-tin sizes is 7.14 mRy.

[f]Energy shift due to different muffin-tin sizes is 9.68 mRy.

als. The LAPW and Madelung energies were fitted to a fourth-order polynomial surfaces in the normal-mode coordinates of the lithium and oxygen (Q_{Li} and Q_{O}). The second derivatives of these energy surfaces at zero displacements are the coefficients of the dynamical matrices. Table II shows the coefficients of the fit for the total energy of $LiNbO_3$ and $LiTaO_3$; all the coefficients for $LiNbO_3$ and $LiTaO_3$ are well constrained except the coefficient of Q_{Li}^2, which means the potential surface describing the displacement of the lithium only could be either a single anharmonic well or a very shallow double well (corresponding to a positive or a negative sign). Linear and cubic terms (e.g., Q and Q^3) are excluded from the fit based on symmetry considerations, and terms that are not along the coordinates calculated; Q_{Li}, Q_{O}, and $Q_{\mathrm{Li,O}}$, are excluded from the fit since they degrade the variances of the quadratic coefficient. These include terms like $Q_{\mathrm{Li}}^3 Q_{\mathrm{O}}$ and $Q_{\mathrm{O}}^3 Q_{\mathrm{Li}}$. The dynamical matrix in units of $\mathrm{Ryd}^2\ \mathrm{\AA}^{-2}$ amu representing the LAPW energies of $LiNbO_3$ and $LiTaO_3$ are

$$D_{\mathrm{LAPW}}(\mathrm{LiNbO_3}) = \begin{pmatrix} D_{\mathrm{Li}} & D_{\mathrm{Li,O}} \\ D_{\mathrm{Li,O}} & D_{\mathrm{O}} \end{pmatrix} = \begin{pmatrix} -0.001 & -0.012 \\ -0.012 & -0.015 \end{pmatrix},$$

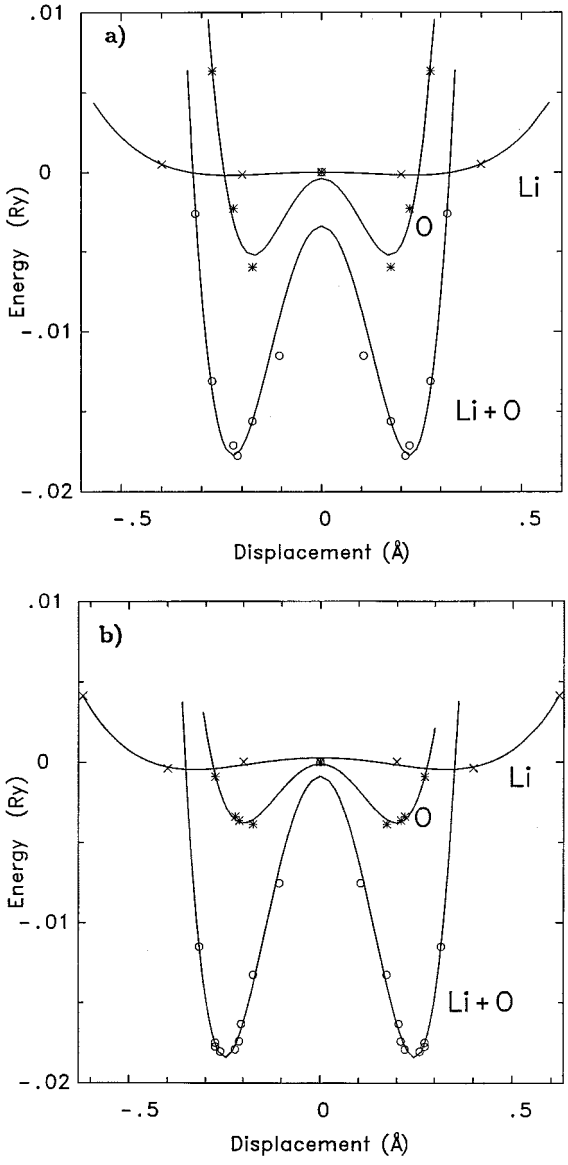

FIG. 2. (a) Potential-energy surfaces of $LiTaO_3$. The upper curves represent displacements of the Li atoms along the soft-mode coordinate, the middle shallow double wells represent displacements of the oxygens alone, and the bottom curves represent the displacements of oxygens and Li atoms along the same coordinate. The curves represent a fourth-order polynomial fit to the data. They were not constrained to go through the zero of energy. The abscissa represents displacement of the oxygen atoms from the paraelectric configuration, in Å. (b) The same for $LiNbO_3$.

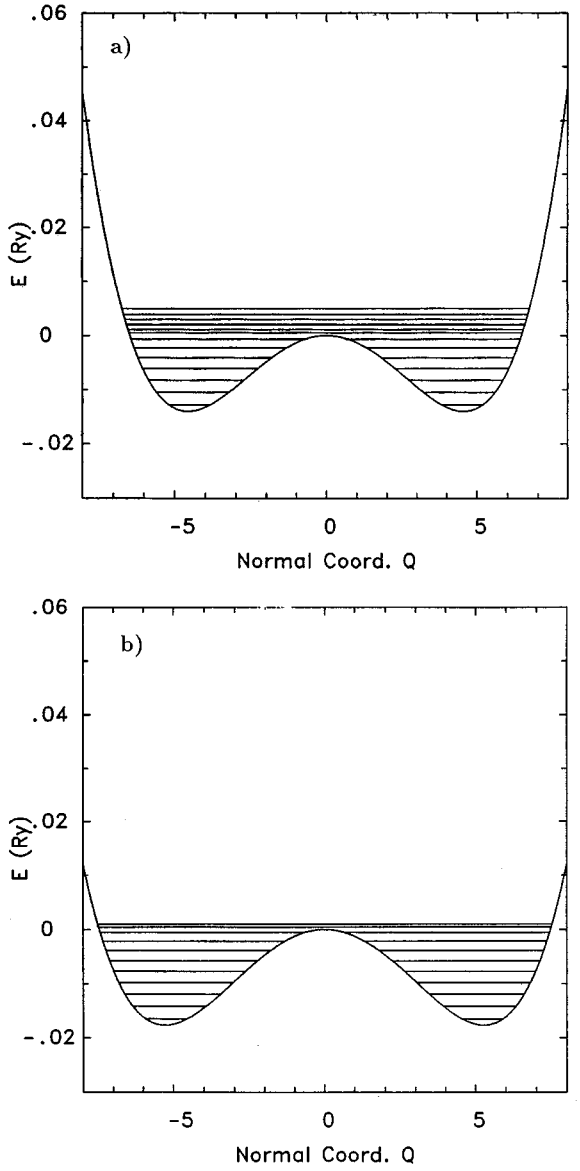

FIG. 3. The energy as a function of normal coordinate, fitted to a quadratic. The lines are the eigenstates for the one-dimensional independent harmonic oscillators. The difference between the ground state and the lowest excited state gives a frequency of 270 cm^{-1} for $LiTaO_3$ and 250 cm^{-1} for $LiNbO_3$. Both are in very good agreement with experimental results. (a) Energy versus normal coordinate for $LiTaO_3$ and (b) The same for $LiNbO_3$.

$$D_{\mathrm{LAPW}}(\mathrm{LiTaO_3}) = \begin{pmatrix} 0.0018 & -0.012 \\ -0.012 & -0.023 \end{pmatrix}.$$

The lithium-only contributions (D_{Li}) are the smallest (an order of magnitude smaller than the rest), the oxygens only contributions are larger, with D_{O} in $LiTaO_3$ larger than $LiNbO_3$.

Whether the origin of lithium and oxygen coupling is Coulombic can be determined by looking at the Madelung contribution to the dynamical matrices. The Madelung energies were calculated using experimental positions and lattice parameters and full ionic charges. The second derivatives at zero displacements, which are the elements in the dynamical matrix, were calculated numerically and are shown in Table II. In the case of $LiNbO_3$ and $LiTaO_3$ the Madelung contributions to the dynamical matrix are

$$D_{\mathrm{MaD}}(\mathrm{LiNbO_3}) = \begin{pmatrix} 0.038 & 0.004 \\ 0.004 & -0.171 \end{pmatrix},$$

$$D_{\mathrm{MaD}}(\mathrm{LiTaO_3}) = \begin{pmatrix} 0.04 & 0.003 \\ 0.003 & -0.162 \end{pmatrix}.$$

As expected, D_{O} has the largest magnitude, followed by D_{Li}. The coupling term between the lithiums and the oxy-

TABLE II. Parameter table for the polynomial fit of the LAPW and Madelung energies. Energies are in Ryd. LAPW $LiNbO_3$ energies are shifted by -16193 Ryd and LAPW $LiTaO_3$ energies by -63395 Ryd.

Coefficient	LAPW energies	Madelung energies
	$LiNbO_3$	
Const	−0.8467(3)	−31.7268(0)
Q_{Li}^2	−0.0005(4)	0.0194(0)
Q_O^2	−0.0075(9)	−0.0857(1)
$Q_{Li}Q_O$	−0.0115(8)	0.0040(0)
$Q_{Li}^2Q_O^2$	0.0017(3)	
Q_{Li}^4	0.0003(1)	
Q_O^4	0.0038(5)	
	$R^2=0.997$	$R^2=0.999$
	$LiTaO_3$	
Const	−0.0800(11)	−31.7714(0)
Q_{Li}^2	0.0009(14)	0.0200(8)
Q_O^2	−0.0117(30)	−0.0812(13)
$Q_{Li}Q_O$	−0.0121(30)	0.0030(8)
$Q_{Li}^2Q_O^2$	0.0010(11)	
Q_{Li}^4	0.0001(3)	
Q_O^4	0.0090(2)	
	$R^2=0.968$	$R^2=0.996$

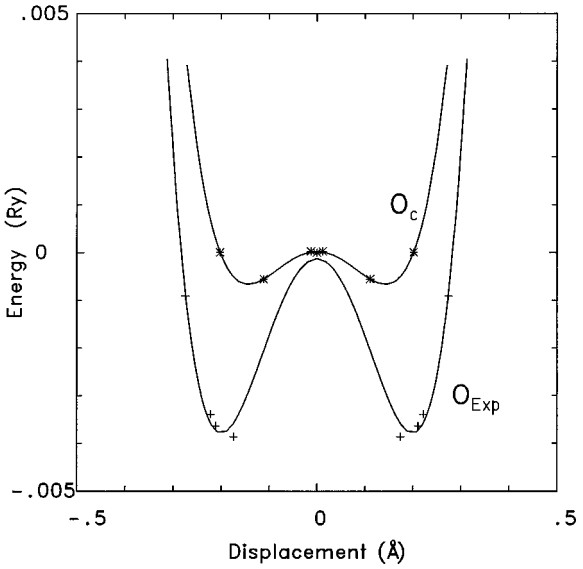

FIG. 4. $LiNbO_3$: Charge density resulting from subtracting the charge density of a configuration in which oxygens only are displaced from the charge density of the full ferroelectric distortion (both lithiums and oxygens are displaced). The scale is from -0.1 to 0.1 electrons per/bohr^3 and the contour interval is 0.002 electrons/bohr^3. No evidence for dynamical covalency effects that would lead to coupling of oxygen and lithium motions are seen.

gens is in fact zero. This means that the origin of the lithium-oxygen coupling is *not* pure Coulombic (Madelung).

Another possibility is the polarization of the oxygens by the lithium displacement, leading to changes in Nb(Ta)-O bonding. The experimental ferroelectric configuration generates an effective dipole at the lithium sites. This dipole field can polarize the oxygens and drive them off center, yielding a ferroelectric distortion. We have plotted the self-consistent charge densities in two configurations; in one only the oxygens are displaced and in the other both the oxygens and the lithiums are displaced. In order to see the effects of displacing the lithiums we subtracted the two charge densities. This is shown in Fig. 4 where the charge density contours are plotted on a scale of -0.1 to 0.1 electrons/bohr^3 and the contour interval is 0.002 electrons/bohr^3. A large dipole is seen at the lithium sites due to the displacement of the lithiums. Little polarization of the oxygens is observed; there is no evidence for any large dynamical covalency effects. We can therefore eliminate the possibility of oxygen-lithium coupling through either Madelung or polarization effects.

Another possible source for the oxygen-lithium coupling is through the crystal structure. It is important to notice that the oxygens move not only along the *c* axis, but rather have sizable displacements along the *a* and *b* axes as well. We have tested the importance of these displacements by moving only the oxygens along the *c* component of the experimental ferroelectric displacement (the polar axis). The resulting energy curve was far shallower than the energy surface that resulted from moving the oxygens only along the experimental soft-mode coordinate. This is shown in Fig. 5 where the upper curve represents the displacements of the oxygens along the polar axis only and the lower, deeper well represents the total energy when displacing the oxygens along the experimental ferroelectric distortion (along *a*, *b*, and *c* axes). The reason for these big energy differences can be seen from Table III, which shows the Ta-O, Nb-O, and Li-O bond lengths. The ionic radii of Li is about 0.6 Å, that of Ta or Nb is about 0.6 Å, and the ionic radii of oxygen is about 1.4 Å,[59] making the sum of each pair (Li-O, Nb-O, and Ta-O) about 2.0 Å. When the oxygens are displaced only along the *c* axis, the oxygen-Nb (Ta) separation becomes only 1.83 (1.86) Å, which is about 0.17 (0.14) Å shorter than

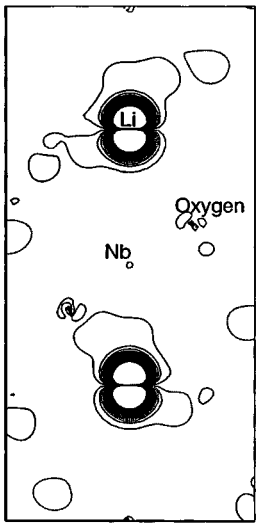

FIG. 5. Total-energy surfaces of $LiNbO_3$ with only oxygens displaced along soft-mode coordinate (lower curve) and with only the oxygens displaced along the *c* axis only (upper curve). The curves are a fourth-order fit to the data. The abscissa represents displacements, in Å, of the oxygens from their paraelectric positions.

TABLE III. Bond length, in Å, of transition-metals–oxygens and Li-oxygens in different configurations. Sum of ionic radii of each pair is about 2 Å.

	Paraelectric	Oxygen only distortions along c axis only	Oxygen only distortions along soft-mode coordinate	Ferroelectric (Li+O)
		$LiTaO_3$		
Li-O	1.99	2.00	1.96	2.04
Ta-O	1.97	1.86	1.91	1.91
		$LiNbO_3$		
Li-O	1.99	2.01	1.96	2.07
Nb-O	1.97	1.83	1.89	1.89

the sum of the ionic radii [about 8 (7)%]. Therefore it is energetically favorable for the oxygens to displace in the *a-b* plane as they move along the *c* axis.

If we now consider the experimental ferroelectric displacement of only the oxygens and the experimental ferroelectric *coupled* displacement of the oxygens and lithiums, displacing the oxygens only results in a Li-O separation that is also shorter than the sum of their ionic radii (Table III). This explains why the wells associated with the oxygen displacements alone are shallower than those obtained with the displacement of *both* the lithiums and oxygens. The origin of the Li-O coupling is therefore the fact that motion of the oxygens alone yields a Li-O distance that is larger than the sum of their ionic radii, resulting in a deeper well for the coupled motion (in which the Li and oxygens move away from each other).

We can therefore conclude that the driving mechanism behind the phase transformation in these systems is the displacement of the oxygens towards the transition-metal atoms. Displacement of the oxygens in the direction of the transition-metal atoms only (the *c* axis) would result in too short Nb- (Ta-) oxygen bonds. The oxygens therefore move also in the plane perpendicular to the *c* axis, toward the lithiums. This shortens the lithium-oxygen bond so that the lithium displacements are coupled with the oxygen motions.

The transition temperature, T_c, cannot be calculated directly from the zone center energetics. In the usual models for ferroelectric phase transitions, T_c is related to the relative strength of the local (on-site) and coupling terms in the energy.[60] Since we find the zone center energetics to be similar, the difference in T_c must be due to differences in the energetics at the zone boundary. In order to understand the origin of the ferroelectric distortion, we next examine the electronic structure of these materials.

B. Electronic structure

One goal of this research is to understand the origin of ferroelectricity in $LiTaO_3$ and $LiNbO_3$ and the difference in T_c from their electronic structure. Figure 6(a) compares the electronic density of states for $LiTaO_3$ and $LiNbO_3$, both at the ferroelectric configuration. The energy scales are lined up with the top of the valence bands at zero energy. It is clear that the total density of states of these two materials is very similar. We can look further at the different contributions to the density of states; Fig. 6(b) compares the partial density of the Ta $5d$ state and the Nb $4d$ state both in the ferroelectric phase. The top of the valence band is composed mostly of oxygen p states. This figure shows a large density of transition-metal d states in the valence band, which means that the oxygen p states in these two materials are hybridized with the d states. The Nb d states have a large peak at the bottom of this band that is missing in the case of the $5d$ states of the Ta atom. The origin of this peak is the fact that the lowest valence bands of $LiNbO_3$ (the bands at about -4.5 eV or -0.35 Ryd) are less dispersive than the lowest

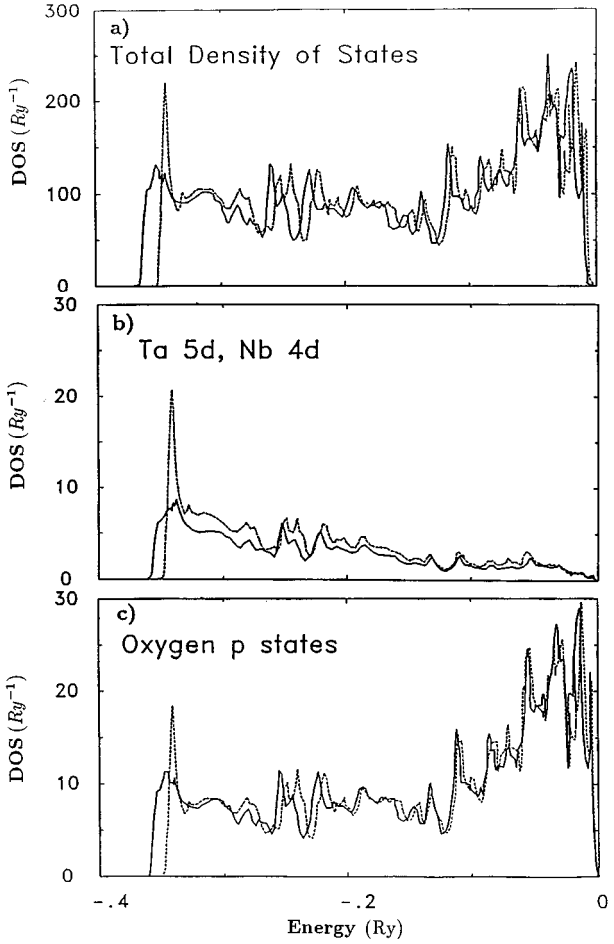

FIG. 6. (a) Electronic density of $LiTaO_3$ (solid line) and $LiNbO_3$ (dashed line), both in the experimental ferroelectric configuration. (b) Density of Ta $5d$ states (solid line) and Nb $4d$ states (dashed line) in the valence band, both the experimental ferroelectric configuration. (c) Oxygen p states of $LiTaO_3$ (solid line) and of $LiNbO_3$ (dashed line) in the valence band, in the ferroelectric phase.

valence bands of $LiTaO_3$. This will be further discussed later. The same conclusion is derived from Fig. 6(c) of the partial density of the oxygen p state of the two materials in the valence band in the ferroelectric structure. Here too, the densities of states are very similar. The same peak at the bottom of the band is seen here for the $LiNbO_3$, which is missing in the valence band of $LiTaO_3$. All three figures that compare the total and partial density of states of the two materials in their ferroelectric phase show large hybridization between the transition-metal d states and the oxygen p states, which is the reason for the oxygen displacements towards the transition-metal atoms.

Next we compare the densities of states in the paraelectric and the ferroelectric phases. Figure 7(a) illustrates the total density of states of $LiNbO_3$ in the paraelectric (solid line) and the ferroelectric (dashed line) phases. The bands in the two phases look similar except that the bands at the ferroelectric phase are slightly wider than the bands at the paraelectric phase. Figure 7(b) compares the Nb $4d$ state in both the paraelectric (solid line) and the ferroelectric (dashed line) phases and Fig. 7(c) shows the Ta $5d$ states in the two configurations. The large peak at the lower part of this band (the peak at about -0.35 Ryd or -4.5 eV) is shifted in the ferroelectric case to higher energies. Figure 7(d) shows the density of oxygen p states of $LiNbO_3$ at the two phases. The peak at the bottom of the band is shifted in the ferroelectric phase from the paraelectric one. These figures indicate that the electronic structure at the paraelectric and the ferroelectric phases are quite similar. Figure 7(e) compares the lithium $2s$ character in the paraelectric and ferroelectric phases. It is evident that the lithium is almost completely ionized and that its electronic distribution does not change during the phase transition.

Figure 8 shows the band structure of $LiNbO_3$ in the ferroelectric state. The band gap is indirect, the top of the valence band is between Γ and Z, and the bottom of the conduction band is at the Γ point. The Brillouin zone for the rhombohedral lattice[61] is illustrated in the inset in the figure. The energy between the Z and the A point was calculated along a straight line between the two points not along the Brillouin zone face for the purpose of comparison with the results of Ching, Gu, and Zu.[62]

The band gap is 3.1 eV, which is about 15% lower than the value obtained from optical measurements of the near stoichiometric sample[63,64] of 3.78 eV. The lithium $2s$ states are separated by 13.6 eV from the oxygen $2s$ states. These bands would not appear in the $LiTaO_3$ band structure since the lithium $2s$ states were treated as core states; these bands are very flat. The oxygen $2s$ are separated by 10 eV from the valence bands. The lowest conduction bands are the Nb $4d$ states for $LiNbO_3$ or Ta $5d$ states for $LiTaO_3$. We have also compared this band structure with Ching, Gu, and Zu[62] who used the orthoganalized linear combination of atomic orbitals (OLCAO) method and got a band gap of 3.56 eV and the bands compare well with our results.

Figures 9(a) and (b) show the band structure for $LiTaO_3$ and $LiNbO_3$, respectively. Each figure shows the ferroelectric (solid line) and the paraelectric (dashed line) phases. The changes observed between the ferroelectric and paraelectric bands are the band gap, which is larger in the ferroelectric phase by about 15% and the bandwidth, especially the conduction band, which is larger in the paraelectric phase.

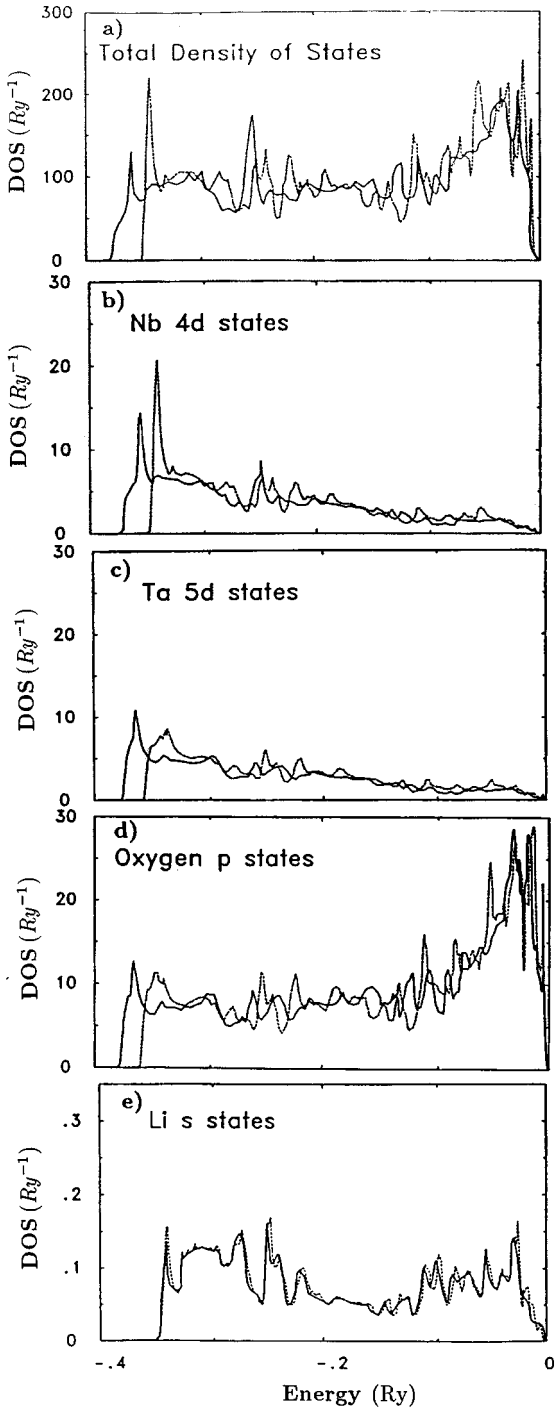

FIG. 7. (a) Electronic density of states for $LiNbO_3$ in the paraelectric (solid line) and ferroelectric (dashed line) configurations. (b) The Nb $4d$ state in the two phases. (c) The $LiTaO_3$ Ta 5d states in the two phases. (d) The $LiNbO_3$ p states on the oxygens in the paraelectric and the ferroelectric phase. (e) The s orbital on the Li atom of $LiNbO_3$ in the two phases. The valence-band top is lined up with the zero of energy.

The band structures of $LiTaO_3$ (dashed line) and $LiNbO_3$ (solid line) both in the ferroelectric phase, are shown in Fig. 10. The only difference between these two band structures is the larger band gap, by about 1 eV (30%), in $LiTaO_3$. The conduction bands are shifted by 1 eV from each other, but otherwise, their structure is almost the same.

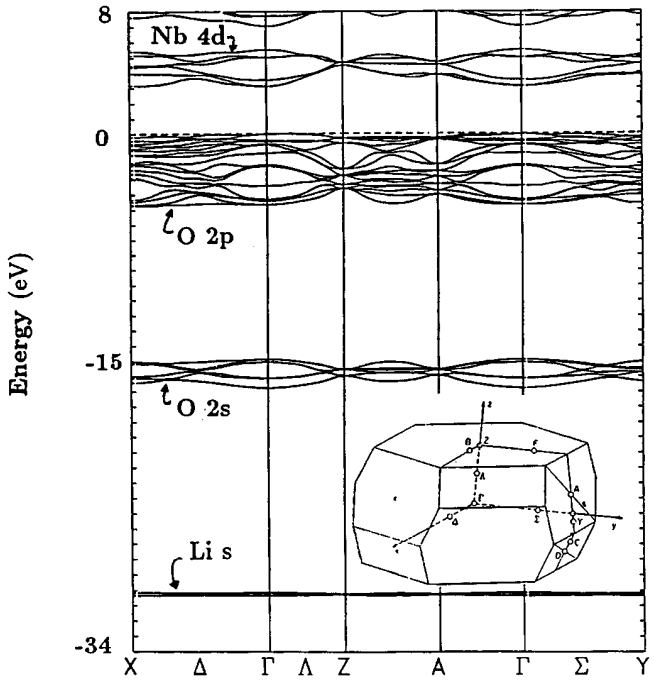

FIG. 8. The band structure of $LiNbO_3$ in the ferroelectric phase. The energy scale is in eV and the Fermi level is shown. The band gap is 3.1 eV. The Li *s* states do not interact with the rest of the bands and are about 16 eV below the oxygen 2*s* states. Inset: The Brillouin zone. Some high symmetry points are illustrated. The energy between the *Z* and the *A* point was calculated along a straight line between the two points. From Ref. 61.

The valence bands are almost identical, which is consistent with the results of the total-energy calculations where the two well depths were found to be very close to each other (within 1.2 mRy of each other) and the fact that the number of valence electrons in the muffin tins in both materials was similar. The only difference that was found between the two electronic structures was in the size of the band gap and the less dispersive nature of one band. The difference in the band gap will have an effect on quantities that include summing over unoccupied states as well as the occupied ones, like the polarizability. This difference will lead to different phonon dispersion in the two materials, and thus to different T_C's. Zone boundary or linear response calculations are necessary to further explore this issue.

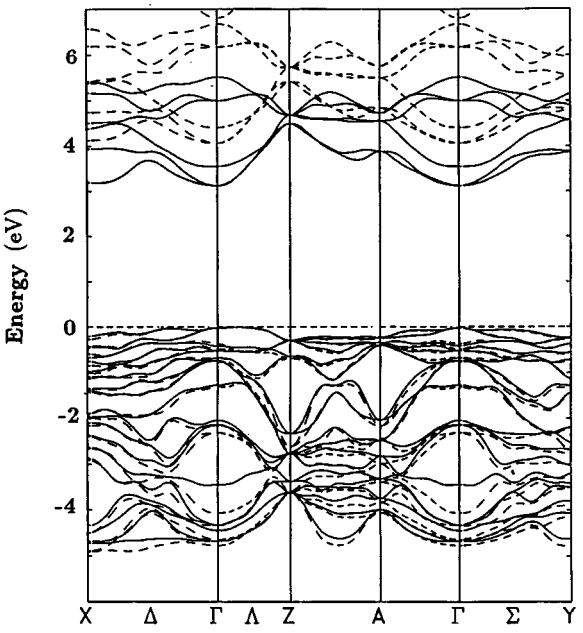

FIG. 10. The band structure of $LiNbO_3$ (solid line) and $LiTaO_3$ (dashed line), both in the ferroelectric structure. The $LiTaO_3$ band gap is larger than the $LiNbO_3$ band gap by about 1 eV. The valence bands of the two materials are almost identical.

C. Comparison to the perovskites

Previously we studied the difference between the self-consistent charge densities and charge densities computed using overlapping ions with the potential induced breathing (PIB) model for both $LiTaO_3$ and $LiNbO_3$ in the ferroelectric phase.[65] In the PIB model, which is a nonempirical ionic model,[66] the charge densities are calculated via a Gordon-Kim-type model,[67] where the ions are allowed to breathe corresponding to changes in the crystal potentials. The comparison indicated large hybridizations between the Ta atoms and the oxygens and between the Nb atoms and its oxygen neighbors and the Li atoms were fully ionized in the self-consistent charge density.

These results are consistent with the energetics and electronic structures results, all pointing to the same conclusion that the driving mechanism behind the ferroelectric instability in the $LiNb(Ta)O_3$ systems is the hybridization between the *d* states on the transition-metal atoms and the $2p$ states on the oxygens. The lithiums are but passive players in the

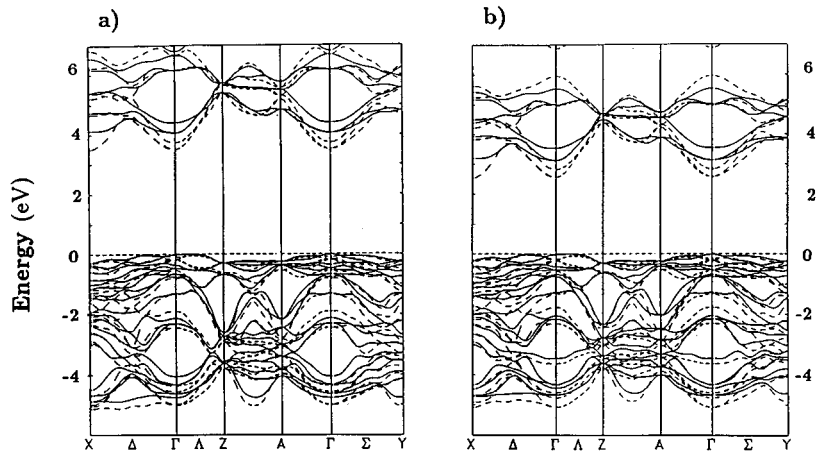

FIG. 9. (a) The band structure of $LiTaO_3$ in the ferroelectric phase (solid line) and the paraelectric (dashed line). Only the valence and the conduction bands are shown. The band gap in the ferroelectric phase is about 4.0 eV, and is decreased in the paraelectric phase by about 15 %. (b) The same for $LiNbO_3$. The gap decreases by about 15% between the ferroelectric and paraelectric phases. No major differences are observed in both systems between the two phases.

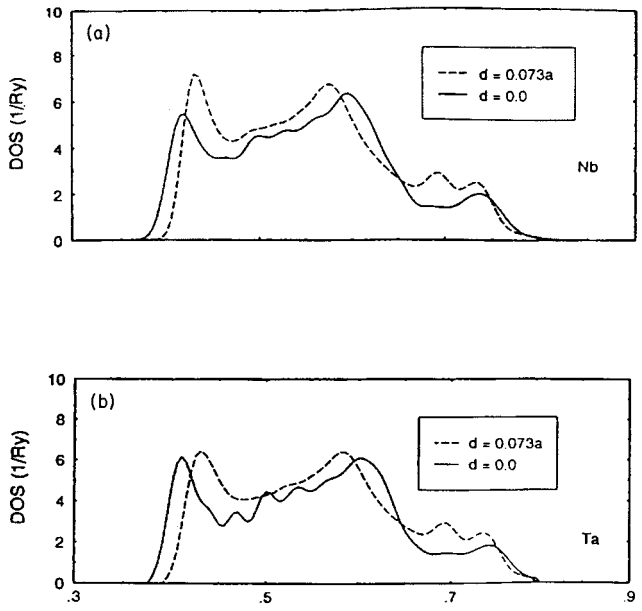

FIG. 11. From LMTO results of $KTaO_3$ and $KNbO_3$, by Postnikov *et al.* (Ref. 29). (a) Local density of states at the Nb site with the Nb undisplaced (solid line) and displaced (dashed line) from its rhombohedral position. The displacement of the Nb atom is exaggerated in order to enhance the trends shown. (b) at the Ta site, under the same conditions. The units are in Ryd for the energies and Ryd^{-1} for the density of states.

ferroelectric instability. This is very similar to the ferroelectric mechanism in the perovskite ferroelectrics, where the oxygen–transition-metal atom hybridization, in addition to the Coulombic long-range interaction, which tends to drive the system off center, overcomes the short-range repulsions, which tend to leave the system in its high-symmetry configuration.

An interesting comparison can be made with the $K(Nb,Ta)O_3$ system; one major difference is the fact that the perovskite $KTaO_3$ is an incipient ferroelectric where $LiTaO_3$ has a high transition temperature. In this sense a qualitative comparison can be made between the two sets of systems, as in both systems the transition temperature is higher in the niobate systems, being zero for $KTaO_3$. This would mean a shallower well for the tantalates, where in the case of $KTaO_3$ the well is apparently lower than the thermal vibrations, as shown by this study for the $Li(Nb,Ta)O_3$ systems and by Postnikov for the $K(Nb,Ta)O_3$ systems.[29]

The electronic structures of the two sets of systems [$LiNb(Ta)O_3$ and $KNb(Ta)O_3$] show a large hybridization between the transition-metal atoms and the oxygens, and the amount of hybridization between the transition metals and the oxygens in the two sets of systems is similar. This can be seen from Fig. 6(b), which shows both the partial density of Nb $4d$ states and that of Ta $5d$ states in the valence bands in the ferroelectric configuration in the $LiNb(Ta)O_3$ systems. We can compare these results to the same densities of states calculated for $KNbO_3$ and $KTaO_3$ by LMTO (Ref. 29) reproduced in Fig. 11. These figures show the Nb (Ta) density of states with the Nb (Ta) atom undisplaced and displaced by $0.073a$ (a being the lattice constant) along the $\langle 111 \rangle$ direction, which is an exaggerated displacement used to enhance the differences between the two phases. We can see that the same trends exists in this picture as in Fig. 6(b) for the Nb (Ta) in $LiNbO_3$ ($LiTaO_3$). The ferroelectric peaks at the bottom of this band are slightly shifted towards higher energies. In both cases there is large hybridization between the transition-metal atoms and the oxygens, but this hybridization does not change much during the transition. This hybridization is essential for the onset of the ferroelectric instability, however, the amount of hybridization in this system does not change much through the phase transition like in other ferroelectrics, e.g., $BaTiO_3$ or $PbTiO_3$.[54]

We find that $LiNbO_3$ and $LiTaO_3$ are almost identical in their electronic behavior. The amount of d character in the valence bands, which is a measure of the hybridization between the transition-metal ions and their oxygen neighbors is very similar. This is in contrast to the conclusion that Ta is less ionic than Nb, reached by Postnikov *et al.* for $K(Ta,Nb)O_3$. This conclusion was based on the smaller transition-metal atom density-of-states peak at the bottom of the valence band, observed in Figs. 11(a) and 11(b). It is seen from Fig. 10 that the origin of this peak is the less dispersive nature of one $LiTaO_3$ band versus $LiNbO_3$.

The similarity between $LiNb(Ta)O_3$ and $KNb(Ta)_3$ is the fact that the driving mechanism for the phase transition in the two systems is oxygen–B-atom hybridization. The difference between the two systems lies in the different structure, which yields a different oxygen–A-atom interaction.

In both $LiNb(Ta)O_3$ and $KNb(Ta)O_3$ the hybridization between the B atoms (the transition metals) and the oxygens causes the oxygens and the B atoms to displace towards each other. In the $LiNb(Ta)O_3$ system the oxygen–B-atom separation is larger than the sum of their ionic radii and the oxygens markedly displace in the a-b plane as they move along the polar axis. This, however, makes the oxygen–A-atom separation larger than the sum of their ionic radii resulting in the coupled oxygen–A-atom motion. This is in contrast to the perovskites where the A site is large enough to allow the oxygens to move towards the A atoms, e.g., $KNbO_3$ where the potassium-oxygen separation in the highest and lowest symmetry structures are about 2.85 and 2.83 Å, respectively, compared with the sum of their ionic radii, which is about 2.78 Å.

It is interesting to note that when doping $KTaO_3$ with lithium atoms (KLT), the system does displace off-center, with a critical concentration of lithiums as small as 2.2%.[68] This could be the result of the lithium ion having a much smaller ionic radii than the potassium with respect to the perovskite structure, being about 0.6 Å for Li and 1.4 Å for K.[59] This would allow the lithiums, driven by Madelung forces, to displace off-center, and due to the large space open to the lithiums in the perovskite structure their amplitudes will be much larger than in the $LiTaO_3$ system, resulting in a dipole field that polarizes the oxygens and distorts them into off-center positions. It should be noted that the phase transition in KLT is significantly different from in a conventional ferroelectric. Azzini *et al.*[69] found that the size of the domains having a homogeneous spontaneous polarization is significantly smaller than the size of the structural domains and DiAntonio *et al.*[70] estimated the size of these domains and determined that this is a ferroelectric transition due to the coincidence of the temperature of the maximum of the

dielectric permittivity with the appearance of other anomalies that are characteristics of a structural transformation.

In the Slater picture of the so-called ''rattling ion,'' the *B* atom lies off center because it is too small to fit into the oxygen octahedra surrounding it. This is in fact the opposite of the picture in the $LiNb(Ta)O_3$ systems where the separation of the oxygens from the Nb (Ta) atoms are smaller (1.9 Å) than the sum of their ionic radii (2 Å). Also, a comparison of the Ta-O distances in $KTaO_3$ and $LiTaO_3$ shows exactly this same effect. In $KTaO_3$, the oxygen octahedra is *larger* than the oxygen octahedra in $LiTaO_3$, and yet, in $KTaO_3$ the *B* atom never displaces to the off-center position, while in $LiTaO_3$, the *B* cation exhibit a ferroelectric distortion.

IV. CONCLUSIONS

It is shown that $LiNbO_3$ and $LiTaO_3$ are very similar in both their electronic structure and energetics. The differences in their well depth are very small, the amount of hybridization in the two materials is similar, and the charge densities are similar. Also, these two materials hardly change their electronic structure during a phase transition. The only difference found between these two systems is the difference in the conduction bands. Zone boundary effects that are not included in this study and this difference in the electronic structure of the two systems are two possible candidates to explain the difference in the transition temperatures of the two systems.

It is demonstrated that contrary to previous models, which emphasized the hopping of the lithium atoms between the three positions as the driving mechanism for the phase transformation, in these systems, no triple-well potential was found for the lithium motion. The deep double wells found are the result of the oxygen displacements towards the transition-metal atoms, which are the result of the hybridization between the two atoms. The wells indicate an order-disorder character for the oxygen. Local changes in the oxygen octahedra are responsible for the lithium displacements from their centrosymmetric sites. The lithiums themselves are passive players in the ferroelectric energetics.

ACKNOWLEDGMENTS

We thank H. Krakauer and D. Singh for the use of the LAPW+LO codes and to H. Krakauer, D. Singh, K. Rabe, and I. Mazin for helpful discussions. This research was supported by the office of Naval Research Grant No. N00014-91-J-1227.

[1] B. T. Matthias and J. P. Remika, Phys. Rev. **76**, 1886 (1949).
[2] A. Glass, Phys. Rev. **172**, 564 (1968).
[3] W. D. Johnston and I. P. Kaminow, Phys. Rev. **168**, 1045 (1970).
[4] J. L. Servion and F. Gervais, Solid State Commun. **31**, 387 (1979).
[5] A. S. Barker and R. Loundon, Phys. Rev. **158**, 433 (1967).
[6] A. S. Barker, A. A. Ballman, and J. A. Ditzenberger, Phys. Rev. B **2**, 4233 (1970).
[7] I. Tomeno and S. Matsumura, J. Phys. Soc. Jpn. **56**, 163 (1987).
[8] A. F. Penna, S. P. S. Porto, and A. S. Chaves, *Light Scattering in Solids*, edited by M. Balkanski, R. C. Leite, and S. P. S Porto (Flammarion, Paris, 1976), p. 980.
[9] A. F. Penna, S. P. S. Porto, and E. Weiner-Avnear, in *Proceedings of the 5th International Conference on Raman Spectroscopy* (H. F. Schulz Verlag, Freiburg, 1976), pp. 634 and 569.
[10] A. F. Penna, A. Chaves, and S. P. S. Porto, Solid State Commun. **19**, 491 (1976).
[11] A. F. Penna, S. P. S. Porto, and E. Wiener-Avnear, Solid State Commun. **23**, 377 (1977).
[12] M. R. Chowdhury, G. E. Peckham, and D. H. Saunderson, J. Phys. C **11**, 1671 (1978).
[13] Y. Okamoto, P. Wang, and J. F. Scott, Phys. Rev. B **32**, 6787 (1985).
[14] M. Zhang and J. F. Scott, Phys. Rev. B **34**, 1880 (1986).
[15] A. Jayaraman and A. A. Ballman, J. Appl. Phys. **60**, 1208 (1986).
[16] C. Raptis, Phys. Rev. B **38**, 10 007 (1988).
[17] G. L. Catchen and D. M. Spaar, Phys. Rev. B **44**, 12 137 (1991).
[18] G. Cheng, B. Hennion, P. Launoist, M. Xianlin, X. Binchao, and J. Yimin, J. Phys. C **5**, 2707 (1993).
[19] Y. Tezuka, S. Shin, and M. Ishigame, Phys. Rev. B **49**, 9312 (1994).
[20] E. J. Samuelson and A. P. Grande, Z. Phys. B **24**, 207 (1976).
[21] C. Prieto, L. Arizmendi, and J. A. Gonzalo, Ferroelectrics **55**, 63 (1984).
[22] I. Tomeno and S. Matsumura, Phys. Rev. B **38**, 606 (1988).
[23] A. C. Nunes, J. D. Axe, and G. Shirane, Ferroelectrics **2**, 291 (1971).
[24] G. A. Samara, Ferroelectrics **73**, 145 (1987).
[25] R. Comes, M. Lambert, and A. Guinier, Solid State Commun. **6**, 715 (1968).
[26] T. P. Dougherty, G. P. Wiederrecht, K. A. Nelson, M. H. Garret, H. P. Jensen, and C. Warde, Science **258**, 770 (1992).
[27] J. P. Sokoloff, L. L. Chase, and D. Rytz, Phys. Rev. B **38**, 597 (1988).
[28] P. J. Edwardson, Phys. Rev. Lett. **63**, 55 (1989).
[29] A. V. Postnikov, T. Neumann, G. Borstel, and M. Methfessel, Phys. Rev. B **48**, 5910 (1993).
[30] A. V. Postnikov, T. Neumann, and G. Borstel, Phys. Rev. B **50**, 758 (1994).
[31] O. Hanske-Petitpierre, Y. Yacoby, J. Mustre de Leon, E. A. Stern, and J. J. Rehr, Phys. Rev. B **44**, 6700 (1991).
[32] R. D. King-Smith and D. Vanderbilt, Phys. Rev. B **49**, 5828 (1994).
[33] W. Zhong, R. D. King-Smith, and D. Vanderbilt, Phys. Rev. B **72**, 3618 (1994).
[34] M. E. Lines, Phys. Rev. **177**, 797 (1969); **177**, 812 (1969); **177**, 819 (1969).
[35] S. C. Abrahams, E. Buehler, W. C. Hamilton, and S. J. Laplaca, J. Phys. Chem. Solids **34**, 521 (1973).
[36] H. Boysen and F. Altorfer, Acta Crystallogr. B **50**, 405 (1994).
[37] D. P. Birnie III, J. Appl. Phys. **69**, 2485 (1991).
[38] D. P. Birnie III, J. Am. Ceram. Soc. **74**, 988 (1991).
[39] D. P. Birnie III, J. Mater. Res. **5**, 1933 (1990).
[40] H. J. Bakker, S. Hunsche, and H. Kurz, Phys. Rev. **B 48**, 9331 (1993).
[41] H. J. Bakker, S. Hunsche, and H. Kurz, Phys. Rev. Lett. **69**, 2823 (1992).

[42] K. Nelson (private communication).
[43] *Theory of the Inhomogeneous Gas*, edited by S. Lundqvist and N. H. March (Plenum, New York, 1983).
[44] W. E. Pickett, Comp. Phys. Rep. **9**, 116 (1989).
[45] O. K. Andersen, Phys. Rev. B **12**, 3060 (1975); S. Wei and H. Krakauer, *ibid.* **11**, 1200 (1985).
[46] L. Hedin and B. I. Lundqvist, J. Phys. C **4**, 2064 (1971).
[47] K. J. Kingma, R. E. Cohen, R. J. Hemley, and H.-K. Mao, Nature **374**, 243 (1995).
[48] L. Stixrude, R. E. Cohen, and D. J. Singh, Phys. Rev. B **50**, 6442 (1994).
[49] L. Stixrude and R. E. Cohen, Geophys. Res. Lett. **22**, 125 (1995).
[50] F. C. Marton and R. E. Cohen, American Mineralogist **79**, 789 (1994).
[51] M. J. Mehl, R. E. Cohen, and H. Krakauer, J. Geophys. Res. **93**, 8009 (1988).
[52] R. E. Cohen, Geophys. Res. Lett. **14**, 1053 (1987).
[53] R. E. Cohen, Comput. Phys. **8**, 34 (1994).
[54] R. E. Cohen and H. Krakauer, Phys. Rev. B **42**, 6416 (1990); R. E. Cohen and H. Krakauer, Ferroelectrics **136**, 65 (1992); R. E. Cohen, Nature **358**, 136 (1992).
[55] D. J. Singh and L. L. Boyer, Ferroelectrics **136**, 95 (1992).
[56] D. Singh, Phys. Rev. B **43**, 6388 (1991).
[57] S. C. Abrahams, J. M. Reddy, and J. L. Bernstein, J. Phys. Chem. Solids **27**, 997 (1966); **27**, 1013 (1966); **27**, 1019 (1966).
[58] R. E. Cohen, Ferroelectrics **153**, 37 (1994).
[59] R. D. Shannon and C. T. Prewitt, Acta Crystallogr. B **25**, 925 (1969).
[60] W. Zhong, D. Vanderbuilt, and K. M Rabe, Phys. Rev. Lett. **73**, 1861 (1994)
[61] GF. Koster, Solid State Physics, edited by F. Seitz and D. Turnball (Academic, New York, 1957), p. 173.
[62] W. Y. Ching, Z. Gu, and Y. Xu, Phys. Rev. B **50**, 1992 (1994).
[63] D. Redfield and W. J. Burke, J. Appl. Phys. **45**, 4566 (1974).
[64] A. Dhar and A. Mansingh, J. Appl. Phys. **68**, 5804 (1990).
[65] I. Inbar and R. E. Cohen, Ferroelectrics **164**, 45 (1995).
[66] Z. Gong and R. E. Cohen, Ferroelectrics **136**, 113 (1992).
[67] R. G. Gordon and Y. S. Kim, J. Chem. Phys. **56**, 3122 (1972).
[68] J. Toulouse, B. E. Vugmeister, and R. Pattnaik, Phys. Rev. Lett. **73**, 3467 (1995).
[69] C. A. Azzini, C. P. Banfi, G. Giolotto, and U. T. Hochli, Phys. Rev. B **43**, 7473 (1991).
[70] P. DiAntonio, B. E. Vugmeister, J. Toulouse, and L. A. Boatner, Phys. Rev. B **47**, 5629 (1993).